RESEARCH ARTICLE

Society For Biomaterials WILEY

Enhancing the soft-tissue integration of dental implant abutments—in vitro study to reveal an optimized microgroove surface design to maximize spreading and alignment of human gingival fibroblasts

Patrick W. Doll[1] | Ayman Husari[2,3] | Ralf Ahrens[1] | Bruno Spindler[4] | Andreas E. Guber[1] | Thorsten Steinberg[2]

[1]Institute of Microstructure Technology (IMT), Karlsruhe Institute of Technology (KIT), Hermann-von-Helmholtz-Platz 1, Eggenstein-Leopoldshafen, Germany

[2]Division of Oral Biotechnology, Center for Dental Medicine, Medical Center-University of Freiburg, Faculty of Medicine, University of Freiburg, Hugstetter Strasse 55, Freiburg, Germany

[3]Department of Orthodontics, Center for Dental Medicine, Medical Center-University of Freiburg, Faculty of Medicine, University of Freiburg, Hugstetter Strasse 55, Freiburg, Germany

[4]MEDTEOR GmbH, Industriestraße 2-4, Oppenau, Germany

Correspondence
Patrick W. Doll, Institute of Microstructure Technology (IMT), Karlsruhe Institute of Technology (KIT), Hermann-von-Helmholtz-Platz 1, 76344 Eggenstein-Leopoldshafen, Germany.
Email: patrick.doll@kit.edu

Abstract

Within this work, we demonstrate the influences of different microgrooved surface topographies on the alignment and spreading of human gingival fibroblast (HGF) cells and present the optimal parameters for an improved soft-tissue integration design for dental implant abutments for the first time. Microgrooves with lateral widths from 2.5 to 75 μm were fabricated by UV-lithography and wet etching on bulk Ti6Al4V ELI material. The microstructured surfaces were compared to polished and ground surfaces as current state of the art. The resulting microtopographies were analyzed using vertical scanning interferometry and scanning electron microscopy. Samples loaded with HGF cells were incubated for 8 and 72 hr and cell orientation, spreading, resulting area, and relative gene expression were analyzed. The effect of contact guidance occurred on all microstructured surfaces yet there is a clear preferable range for the lateral widths of the microgrooves between approx. 11.5 and 13.9 μm and depths between 1.6 and 2.4 μm for an abutment surface design, where cell orientation and spreading maximizes. For structures larger than 30 μm, cell orientation, spreading and even gene expression of intercellular adhesion molecule-1 and yes-associated protein decrease.

KEYWORDS

contact guidance, human gingival fibroblasts, microgrooves, Ti6Al4V, UV-lithography

1 | INTRODUCTION

Implant associated infections are a major problem in the treatment of edentulous patients.[1,2] Due to bacterial infections or metal ion release based inflammations, the so-called peri-implantitis describes the inflammation of the peri-implant soft and hard tissues often connected with aggressive bone necrosis.[3,4] Studies have shown that especially the soft-tissue connection at the implant abutment/soft-tissue interface plays a crucial role for the successful integration of the whole implant system.[5,6] If the attachment of the surrounding gingival tissue is insufficient, no tight sealing protects the underlying bone from the negative bacterial influences of the oral cavity.[5-7]

The moment an implant abutment is inserted into the oral cavity bacteria and eukaryotic cells conquer for the settlement on the surface

and for the integration of the implant.[6] This so-called "race for the surface" describes an evolutionary fight for the alloplastic material surface.[6,8,9] If bacteria can successfully adhere to the surface and produce a biofilm of a critical size the successful integration of the surface by eukaryotic cells like gingival fibroblast or endothelia cells into the surrounding tissue cannot be achieved anymore.[6,9] If the surface is covered by a dense layer of eukaryotic cells and successfully integrated into the surrounding tissue instead, bacteria cannot build a biofilm on the surface and cannot get to the underlying bone and cause infections.[6,9] This race for the surface takes place for every alloplastic material inserted into the human body, but especially the oral cavity with its enormous amount of microorganisms is a perfect example and measures have to be taken to change the outcome and to reduce possible post-operative complications.[9]

On the one hand, there have been various attempts to reduce the initial adhesion and biofilm formation of microorganisms by surface structuring or surface modifications.[10-12] On the other hand, the soft-tissue integration can be enhanced by an effect called contact guidance.[13] Eukaryotic cells as well as microorganisms follow micro- and nanotopological features on a surface and orient themselves with the structure orientation.[10,13,14] This effect was described more than 75 years ago for example, by Weis where he found that cells orient and align to underlying substrate features.[15] Especially the works of Brunette et al in 1990s has increased the interest in the effect and the underlying microstructures.[13,16,17] Many other studies since then have focused on the effect of contact guidance and the overall sizes of the microstructures termed "microgrooves."[18-27] In summary, it has been reported that cells align with present grooves in a wide range of only a few dozen nm up to three digit micrometers. As much information is available in literature, the optimal lateral width has not yet been reported in detail nor is the exact mechanism behind the effect adequately solved. Especially on bulk material like the implant abutment material Ti6Al4V ELI the effect of contact guidance has only been reported insufficiently at all. One possible reason for the still not fully understood mechanism and influencing parameters are the limitations in microfabrication and the availability of different cross-sectional topographies in the micrometer range.[28]

Within this work, we describe the optimal range of lateral structure widths for contact guidance of human gingival fibroblast (HGF) on the dental abutment material Ti6Al4V ELI as well as the influences on cell orientation, spreading, area, and relative gene expression.

2 | MATERIALS AND METHODS

2.1 | Sample material

Medical titanium grade 23 (Ti6Al4V ELI) was used for the experiments and preparation was performed as described elsewhere.[29] In summary, 2 mm thick disks have been cut out of a bar with a diameter of 8 mm by wire erosion. A grinding step and a following mechanical/chemical polishing procedure result in adequately even and flat surfaces with very low average roughness values, which are suitable for UV-lithographic microfabrication. As unstructured reference-samples polished as well as ground samples were used.

2.2 | UV-Lithography

2.2.1 | Coating

Samples have been coated with a positive tone photoresist (AZ 1505, Merck Performance Materials GmbH, Germany) by spincoating (ST50, ATM GmbH, Germany) using a rotation-speed of 1,000 rpm, an acceleration ramp of 1,500 rpm/s and a time of 60 s, what resulted in an average photoresist thickness of approx. 1 µm. Afterwards the samples have been softbaked on a hotplate at 90°C for 5 min to evaporate the remaining solvent.

2.2.2 | Exposure

Before the main exposure, the edge bead was removed by a first exposure and development step. The main exposure was carried out using an individually designed chromium/glass mask (Delta mask BV, Netherlands). For the exposure lateral line widths of 2.5, 5, 7.5, 10, 15, 20, 25, 30, 50, and 75 µm at a duty cycle of 50% were used. Exposure was carried out in a contact exposure setup for 4.3 s at an intensity of the flood exposure system of approx. 23.5 mW/cm^2 resulting in an average applied dose of 100 mJ/cm^2.

2.2.3 | Development

After exposure samples have been manually developed in a mixture of AZ400K and DI-water (1:4) for 2 min within a glass beaker placed on a shaking plate at 150 rpm.

2.2.4 | Etching

Wet etching has been performed with a hydrofluoric acid (HF) based etchant. A mixture of HF (5%) and H_2O_2 (30%) was used. The etching time depended on the lateral structure width of the applied and structured photoresist layer as it is described by Equation (1). Since a mask with a duty cycle of 50% was used the resulting ridge to groove ratio after the etching process is not equal due to the isotropic etching and the resulting underetching of the photoresist. Choosing an etching time t_{etch} to obtain a 50% underetching results in a ridge to gap ratio of 1–3.

$$t_{etch} = \frac{d_s}{c_{etch}} \cdot u_e. \tag{1}$$

The etching speed c_{etch} for the etchant was in a range of 2.5 and 3.5 µm/min and was determined for each new mixture of etchant. Within Equation (1) d_s represent the lateral structure width of the structured photoresist and u_e a factor for the degree of underetching.

2.3 | Surface characterization

2.3.1 | Scanning electron microscopy

Samples have been analyzed by scanning electron microscopy (SEM) (Supra 60 VP, Zeiss AG, Germany) at working distances between 1.5 and 6 mm using a secondary electron (SE2) detector. An extra high tension (EHT) between 1.5 and 10 kV was used. The samples covered with cells were sputter-coated with a 15 nm thick silver layer. Six non-overlapping images have been taken per sample in an equidistant arrangement covering the center of the sample.

2.3.2 | Vertical scanning interferometry

3D surface measurements were performed using vertical scanning interferometry (VSI) (Contour GT, Bruker Corp., MA). The field of view was set to 1.7 x 1.3 mm^2 and additionally 170 x 130 μm^2 depending of the objective used. Three samples per parameter for the flat reference samples as well as the structured samples have been measured at three individual positions per sample.

2.4 | Cells and culture condition

HGF cell line has been extracted from a patient earlier and was kept in long time cryo storage. The cells were used at passage 5 for all experiments and cultivated in 95% humidified atmosphere with 5% CO_2 at 37°C. The culture medium consisted of Dulbecco's Mofied Eagle Medium (Life Technologies) supplemented with 10% fetal calf serum (Biochrom), 2 mM L-alanyl-L-glutamine (Invitrogen) and 0.1 mg/ml kanamycin (Sigma-Aldrich). Donating patients' agreement was obtained according to the Helsinki Declaration and the protocol was authorized by the ethics committee of the Albert-Ludwigs-University, Freiburg, Germany (Votum No. 411/08; Date November 20, 2008). The surfaces were sterilized in 80% ethanol twice and rinsed with phosphate buffered saline (PBS) before use. 1×10^4 HGF cells were seeded on a surface and put in an incubator (37°C, 5% CO_2).

2.5 | Indirect immunofluorescence

After 8 and 72 h of incubation, the cells on the surfaces were fixed with 3.8% paraformaldehyde solution (PFA, Carl Roth, Germany), rinsed with PBS and permeabilized with blocking solution (5% BSA and 0.1% Tween-X-100 in PBS). For actin cytoskeleton staining, specimens were incubated with Phalloidin-Alexa488 (Thermo Fisher scientific). Nuclear staining was performed with DAPI (Thermo fisher scientific). Finally, samples were embedded in mounting medium (Fluoromount G, Biozol Diagnostica, Germany). Indirect immunofluorescence (IIF) images were acquired with a Keyence BZ-9000 fluorescence microscope (KEYENCE GmbH, Germany).

2.6 | RNA isolation and quantitative real time PCR

To gain information about intracellular actions, different proteins have been analyzed. Finely ground, 7.5, 15, 30, and 75 μm period samples were used. Five groups were chosen after initial analyzation of cell orientation to cover the whole range of lateral widths.

The relative gene expression of the co-transcriptional activator yes-associated protein (YAP, ReSeq# PPH13459A-200) and the intercellular adhesion molecule 1 (ICAM-1, RefSeq# PPH00640F-200) were assessed on mRNA level by semi quantitative real-time RT-PCR. After 8 and 72 hr HGFs culture period, the total RNA was isolated from HGFs, using the RNeasy plus mini kit (Qiagen, Germany). RNA concentration and integrity was measured by a QIAxpert instrument (Qiagen). Synthesis of cDNA was performed with 100 ng mRNA using RevertAid First Strand cDNA Synthesis Kit (Thermo Fisher Scientific) according to the manufacturer's protocol using a C1000 Thermal Cycler (Bio-Rad). Real-time PCR reactions were carried out with the CFX96-Real-time PCR Detection System (Bio-Rad Laboratories) using RT2 SYBR Green qPCR Master Mix (Qiagen), and cDNA equivalent to 10 ng of total mRNA. 1 μl pre-dispensed gene specific primer pairs were pipetted into each well containing 24 μl of the master mix. Relative mRNA expression of YAP and ICAM-1 was normalized to the housekeeping genes ribosomal protein RPL13a (RPL13A; RefSeq# NM_012423, Qiagen), and glyceraldehyde-3 phosphate dehydrogenase (GAPDH; RefSeq# NM_001256799, Qiagen). Data were collected and analyzed using CFX96 Manager Software version 1.0 (Bio-Rad).

2.7 | Cell orientation, spreading, and area

Cell orientation angles, spreading and the resulting areas have been determined using SEM images and the open source program ImageJ. The orientation of the main cell axis (long axis) of each cell was compared to the unidirectional structure orientation. An angle of 0° implies that a cell is aligned parallel along the microgrooves, while an angle of 90° represents a perpendicular orientation to the structure direction. The range of possible orientation angles was set from 0° to 90° since movement direction cannot clearly be determined.

Cell spreading indices were acquired for each individual recognizable cell on the captured SEM-images by measuring long and short axis of the cells. The spreading index is defined as ratio of long axis to short axis. It gives information about the degree of elongation and can indicate the current cell state (apoptosis/movement/proliferation etc.). A minimum possible spreading index of 1, where the long axis is as short as the short axis, indicates a rounded cell shape what might (yet not necessarily) indicate an idle state or even an early stage of cell apoptosis. Indices between approx. 1.25 and 3 might mainly indicate cell movement while indices larger than 3 indicate an elongated spindle like cell.

Cell area was further determined with the program ImageJ after removing the background out of each SEM image leaving only the

cells. Transferred to a two-color bitmap the areas covered and uncovered by cells were determined.

2.8 | Statistical analysis

For statistical evaluation, the software OriginPro 2018b (OriginLab Corporation, MA) was used. Since cell behavior was found to be linked to the surface geometry we worked with four samples for the different lateral structure periods for incubation times 8 and 72 hr. All data was acquired out of at least three individual images per sample. For each parameter discussed, an average of approx. 440 individual HGF cells was analyzed to acquire cell orientation and cell spreading. For gene expression a total of 10 samples (N = 10) per protein and time point (8 and 72 hr each) have been used for PCR-analysis. Statistical differences have been analyzed using one way ANOVA and Turkey's test to show individual differences. Significance level was set to $p < .05$.

3 | RESULTS

3.1 | Surface characterization

Table 1 displays statistical results of interferometric measurements of the microgrooved surfaces depending on the lateral structure width. The theoretical ridge to groove ratio was set to 1:3 through wet etching time (Equation (1)). Resulting deviations mainly result through the manual wet-etching process. The analysis of the average surface roughness on the etched surfaces revealed values of approx. 0.848 ± 0.124 μm using optical interferometry and field of views of 0.17 x 0.13 mm^2. The polished surfaces have average surface roughness values of <2 nm while the ground surfaces show average roughness values of approx. 52 ± 12 nm for the finely ground and 83 ± 23 nm for the coarse ground surfaces respectively.

TABLE 1 Results of interferometric measurements of the fabricated microgroove structures. Ridge to groove ratio is set to 1:3 by wet-etching. Depth is also a result from isotropic etching. The structures are scaled linearly in width and depth. Deviations mainly result through manual wet etching and increase with lateral size and etching time

Width (μm)	Ridge (μm)	Groove (μm)	Depth (μm)
2.5	0.9 ± 0.2	4.1 ± 0.2	0.4 ± 0.2
5	2.8 ± 0.3	7.3 ± 0.4	0.9 ± 0.1
7.5	3.5 ± 0.4	11.5 ± 0.3	1.6 ± 0.1
10	6.1 ± 0.3	13.9 ± 0.3	2.4 ± 0.1
15	8.2 ± 1.2	21.9 ± 1.2	3.0 ± 0.1
20	8.7 ± 1.4	31.3 ± 1.4	3.2 ± 0.2
25	9.8 ± 1.2	40.2 ± 1.3	4.0 ± 0.2
30	10.8 ± 1.1	49.6 ± 0.9	4.6 ± 0.3
50	26.2 ± 1.7	73.9 ± 1.7	8.7 ± 0.3
75	40.2 ± 4.2	109.3 ± 1.3	9.9 ± 1.2

3.2 | Cell orientation

The results of cell orientation analysis are shown in Figure 1. As expected, there is no preferred cell orientation on unstructured flat surfaces (polished or ground) after 8 hr of incubation. In contrast to the flat and unstructured surfaces a significant preferred cell orientation can be observed for all microstructured surfaces. Even structures smaller than the average cell size of approx. 10 μm are recognized by the cells and have an effect on the cell orientation. This can be clearly seen for the smallest lateral structure width, which was used within this work (2.5 μm). Cells preferably lie on the top of the ridges being only partly in contact with the bottom of the grooves as it could be observed from SEM analysis, yet they orient themselves by the
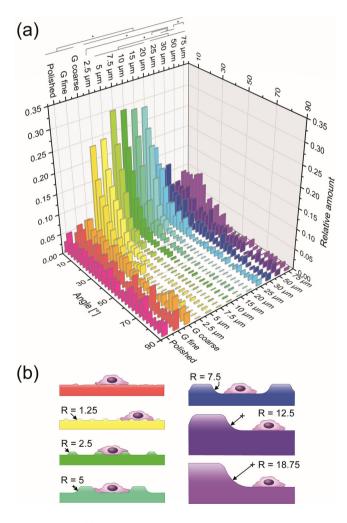

FIGURE 1 (a) Diagram showing the alignment of HGF-cells on different surfaces. While there is no preferred orientation on polished or ground samples the effect of contact guidance can be observed on all microstructured surfaces. The maximum alignment can be found between 7.5 and 20 μm. For widths larger than 20 μm cell alignment is decreased and the amount of other orientations is increased. (b) Schematic drawing to visualize the sizes of grooves and cells with indications of the present curvature. HGF, human gingival fibroblast

recognized surface topological features. In this case, the average height of the microgrooves is only 0.4 ± 0.2 μm.

If the structures are larger in lateral width as well as in height, the amount of oriented cells and the orientation strength is increased respectively. As it can be seen in Figure 1a, the maximum cell orientation can be found for lateral structure widths between approx. 7.5 and 20 μm (mask size). For structure, widths larger than 20 μm a drop in cell alignment can be observed. As indicated in Figure 1b the average cell size is then much smaller than the size of the grooves. This means that cells can only recognize the structure walls and align themselves accordingly at the sidewalls/edges of the ridges. What also can be observed is the fact that more cells take various other orientation angles if the lateral structure width is larger than 20 μm. While many cells are aligned along the microgrooves for larger as well as for smaller lateral widths many cells even orient perpendicular to the structure orientation more or less completely ignoring the underlying microgroove topography. This behavior becomes visible for the largest lateral structure width of 75 μm. Here some cells can still be found oriented along the structures, yet many cells even stay in a rounded cell shaped not orienting themselves with the structures at all. It also can be recognized that many cells ignore the larger microgrooves completely, moving or settling down even on the sidewalls of the ridges. This indicates that there might be a critical structure curvature cells are able to recognize as a groove side wall as also reported recently by Piechot et al.[30]

3.3 | Cell spreading

The results of cell spreading analysis are shown in Figure 2. It also shows nearly the same ranges of lateral structure widths take effect like in cell orientation analysis. For the reference surfaces many cells show indices between 1.25 and 3 indicating cell movement. Many cells even show indices of approx. 1 what might indicate an idle state or even an early stage of cell apoptosis. If there are microgrooves

present on the structures it can be observed that a larger number of cells show an increased spreading index. The spreading index increases with increasing lateral structure width and shows maximum values for approx. The same lateral structure widths where cell orientation was also found to be maximum (7.5–20 μm). If the structures are larger than 20 μm the cell spreading decreased again indicating higher movement and also higher amount of cells in an early stage of apoptosis.

3.4 | Cell area

Corresponding to cell orientation and spreading, the areas covered by cells also show same tendencies (see Figure 3). While the polished and ground sample show slightly lower covered areas, as indicated in Figure 3 a and b, the largest surface coverage can be found between 7.5 and 20 μm. The SEM and immunofluorescence images in Figure 3 exemplarily show this behavior for the finely ground and the microstructured surfaces. Figure 3 a bottom shows the 7.5 μm period microgrooves and Figure 3 b bottom shows the 20 μm period microgrooves. Yet there can be found no statistical significant difference in covered area between the structured surfaces and the reference surfaces. Only if the lateral structure width is as large as 75 μm a statistical significance to the structured samples can be found (p < .05) (data not shown). After 72 hr of incubation no significant differences between structured and the unstructured surfaces can be found and cells grew over the whole surface. Though the cells on the unstructured surface show a certain degree of random orientations (see Figure 3c).

3.5 | PCR results

Analysis of the synthesis and segregation of the adhesion protein ICAM-1 reveals the already mentioned tendencies further (see Figure 4). For small lateral widths (7.5 μm) as well as for the reference
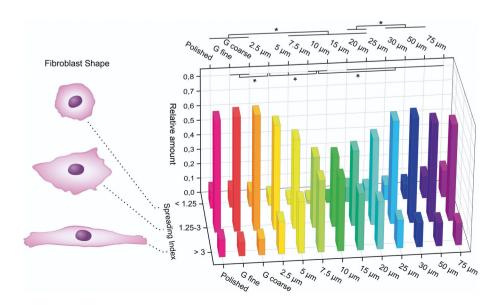

FIGURE 2 Results of cell spreading analysis. For polished and ground surfaces many cells show indices between 1.25 and 3 indicating cell movement. Most elongated cells and least cells with indices <1.25 are found on 7.5 and 10 μm structures
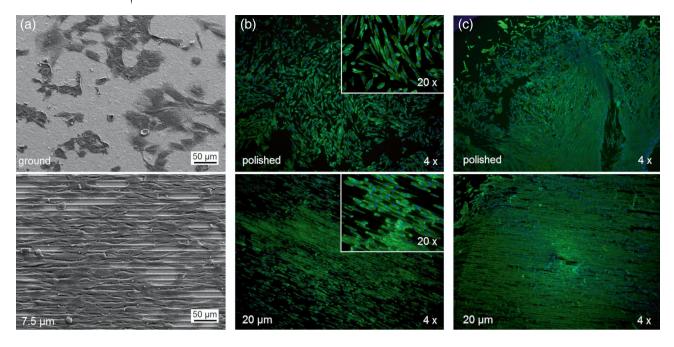
FIGURE 3 Scanning electron micrographs and immunofluorescence images of unstructured and microstructured surfaces. (a, top) A finely ground surface showing randomly oriented HGF-cells after 8 hr. (a, bottom) 7.5 μm microstructured surfaces showing a denser coverage and oriented cells. (b, top) Immunofluorescence image of a polished surface after 8 hr. (b, bottom) 20 μm structures showing aligned cells. (c) Polished and 20 μm surfaces after 72 hr of incubation. The polished surface shows a higher degree of randomness while the cells on the 20 μm structure are unidirectional aligned to the grooves. HGF, human gingival fibroblast
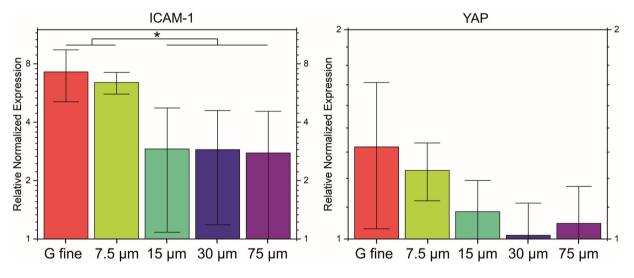

FIGURE 4 Results of RNA isolation and PCR of selected samples. There can be found up regulated ICAM-1 levels on the finely ground and 7.5 μm samples ($p < .05$). The expression of YAP shows a falling trend as the lateral structure width gets larger. Downregulation of YAP inhibits proliferation and induces apoptosis. YAP, yes-associated protein

(ground) surface there can be found a higher relative gene expression than on the larger lateral structure widths, indicating higher cell–cell adhesion, cell–cell interaction and less apoptosis. After 72 hr of incubation, no major differences can be detected anymore (data not shown). For YAP, which is an indicator of cell proliferation and inhibition of apoptosis, the ground samples as well as the small lateral width of 7.5 μm reveal the highest levels. If the lateral widths get larger, a drop can be observed in the synthesis of YAP.

4 | DISCUSSION

The presented results show that a microstructured surface influences the behavior of HGF-cells drastically. Within the observations and limitations of our experiments, this behavior was observed to be intrinsically linked from the cells themselves. Cells simply react to the presented surface topography. In contrast to previously published studies, we provide detailed information of the optimal range and

further information of the occurrence of distinct effects within the contact guidance of HGF-cells.

Within this study, the effect of contact guidance was observed on all microgrooved surfaces, indicating that unidirectional features in a broad range of sizes can be recognized by the cells to align themselves along the structure geometry. While these observations are in line with previous published studies, a detailed look at different lateral sizes of the microgrooves reveals large differences in the strength of the contact guidance effect.

The cells orientation angles show if the cells react and align themselves with the underlying microstructures. In general, the alignment of cells can be very useful for implant surfaces to guide the cells toward a preferred direction or otherwise inhibit the movement in other directions. In wound healing, cell orientation and movement are a very important mechanisms for the overall integration of the alloplastic implant within the surrounding tissues.[31,32] For dental implants or implant abutments this means that a tight cuff of soft-tissue around the implant neck or the subgingival part of the abutment can be realized faster on a microstructured surface than on an unstructured surface. The optimum range for the lateral size of microgrooves can be clearly entitled in the range between 7.5 and 20 μm (mask size) with corresponding depths of only 1.6–3.2 μm.

In our experiments, the cells are placed manually, in the wound healing process they are getting to the surface via the blood stream or intrude via the wound edges and firstly need to order themselves, communicate, form tight cell–cell junctions and build up groups of orientation and elongate in the further growth process.[32,33] Within the beginning of this process, many cells with different orientations are present until larger groups with similar orientations are building up. For longer incubation (72 hr), larger groups of cells with the same orientation can also be found on flat and unstructured surfaces (see Figure 3c), yet they still differ in their average orientation angles and show more randomness between the subdivisions of the oriented cell groups. In case of microstructured surfaces for said parameters, a denser layer of unidirectional oriented cells can be observed already after 8 hr of incubation and after 72 hr a complete coverage of the whole surface was found.

These results are further confirmed if the cell spreading is analyzed. While spreading indices of about 1 are results of cells in a rounded shape, larger values imply cell movement and even larger values of above approx. Three can indicate an elongated native spindle like cell shape as it is needed for target tissue homeostasis. In the results of cell spreading analysis very interesting correlations can be recognized since spreading change as the lateral sizes of the microstructures changes respectively. It can be observed that on the unstructured surfaces as well as on small (≤5 μm) and larger microgrooves (≥15 μm) the movement aspect of the cells (spreading indices >1.25 and <3) dominates, so we can assume that mainly movement occurs. On the other hand, on structures with widths of 7.5 and 10 μm the elongation is dominating compared to the movement aspect, what might, yet not necessarily, indicate increased proliferation on these structures.

These results show that the term contact guidance is a delicate topic. On the one hand aligned cells can indicate cell movement and on the other hand, cell-settling and proliferation. This is particularly interesting since the effect of contact guidance was found for a broad range of lateral structure widths within the present study as well as in literature.[18-27] Yet with the presented results, these previous findings might be partly seen as indication of movement along surface features rather than an optimized effect for proliferation. As a consequence, a detailed view and a differentiation between movement and settlement/proliferation within the contact guidance effect should be introduced in future works.

These implications are further confirmed if the gene expression is analyzed. The interaction between cells and their milieu is known to influence the cell behavioral processes, such as apoptosis, proliferation, and differentiation.[14,34] Transcription factors and their coregulatory molecules like YAP belong to these molecules. The transcription of YAP was found increased on 7.5 μm compared to the other structured samples indicating more proliferation and less apoptosis. For larger lateral structures there was found less YAP-expression and corresponding higher apoptosis. The ICAM-1 is a membrane-bound molecule involved in cell–cell adhesive interactions and signal transduction.[35] Surfaces with 7.5 μm were able to induce the ICAM-1 expression on the cell surface of HGFs. Larger structures showed significantly lower amount of ICAM-1 indicating less cell–cell interaction. Compared to a flat reference, where both, ICAM-1 and YAP, do not significantly differ to the 7.5 μm period microstructure, we can find faster orientation and spreading on the structured surface. On the larger lateral structure width instead, a higher mobility can be observed.

The presented results clearly demonstrate a possible way to enhance soft-tissue integration by applying microgrooves to the implant surfaces. With the presented microstructures an accelerated growth and faster coverage of an implant surface can be realized. This acceleration of orientation and settlement process of HGF cells changes the outcome of the race for the surface toward the integration aspect of eukaryotic cells and reduce the risks of biofilm formation.

While this study highlighted microgrooves on flat Ti6Al4V samples, one challenge is the transfer of such structures to 3D shaped implants. A possible method can be a rotational lithography technique as we presented previously.[36]

5 | CONCLUSION

We demonstrated the optimal lateral sizes for microgrooves to have maximal effect on cell alignment, cell spreading and growth of HGF-cells for the first time. While flat and unstructured surfaces show no alignment after early attachment (8 hr) all structured surfaces tested within this study showed an immediate influence on cell orientation. Within this work, we found that on 7.5 and 10 μm (mask width) microgrooves are optimal for contact guidance of HGF-cells. When the microgrooves become larger and especially structures larger than

20 μm, the alignment strength, the spreading as well as gene expression of ICAM-1 and YAP are decreased. While this behavior occurs for short-term incubation, no large differences can be found after 72 hr of incubation.

CONFLICT OF INTEREST

The authors declare that they have no known competing financial interests.

DATA AVAILABILITY STATEMENT

Data available on request from the authors.

REFERENCES

1. Donelli G, ed. *Biofilm-Based Healthcare-Associated Infections*. Vol I. Cham, Switzerland: Springer International Publishing; 2015.
2. Dreyer H, Grischke J, Tiede C, et al. Epidemiology and risk factors of peri-implantitis: a systematic review. *J Periodontal Res*. 2018;*53*: 657-681.
3. Berglundh T, Armitage G, Araujo MG, et al. Peri-implant diseases and conditions: consensus report of workgroup 4 of the 2017 world workshop on the classification of periodontal and peri-implant diseases and conditions. *J Clin Periodontol*. 2018;*45*(suppl 20):286-291.
4. Fretwurst T, Buzanich G, Nahles S, Woelber JP, Riesemeier H, Nelson K. Metal elements in tissue with dental peri-implantitis: a pilot study. *Clin Oral Implants Res*. 2016;*27*:1178-1186.
5. Chien H-H, Schroering RL, Prasad HS, Tatakis DN. Effects of a new implant abutment design on peri-implant soft tissues. *J Oral Implantol*. 2014;*40*:581-588.
6. Zhao B, van der Mei HC, Subbiahdoss G, et al. Soft tissue integration versus early biofilm formation on different dental implant materials. *Dent Mater*. 2014;*30*:716-727.
7. Zijnge V, van Leeuwen MBM, Degener JE, et al. Oral biofilm architecture on natural teeth. *PLoS ONE*. 2010;*5*:e9321.
8. Gristina AG, Naylor PT, Myrvik Q. The race for the surface: microbes, tissue cells, and biomaterials. In: Switalski L, Höök M, Beachey E, eds. *Molecular Mechanisms of Microbial Adhesion*. New York: Springer; 1989:177-211.
9. Martínez-Pérez M, Conde A, Arenas M-A, et al. The "race for the surface" experimentally studied: in vitro assessment of staphylococcus spp. adhesion and preosteoblastic cells integration to doped Ti-6Al-4V alloys. *Colloids Surf B Biointerfaces*. 2019;*173*:876-883.
10. Doll PW, Al-Ahmad A, Bacher A, et al. Fabrication of silicon nanopillar arrays by electron beam lithography and reactive ion etching for advanced bacterial adhesion studies. *Mater Res Express*. 2019;*6*: 65402.
11. P.W. Doll, M. Wolf, M. Guttmann, R. Thelen, R. Ahrens, B. Spindler, A. E. Guber, A. Al-Ahmad, Initial bacterial adhesion properties of anodically oxidized Ti6Al4V, Paper presented at: Conference proceedings Annual International Conference of the IEEE Engineering in Medicine and Biology Society. IEEE Engineering in Medicine and Biology Society Annual Conference 2019 (2019) 6476–6480.
12. Luan Y, Liu S, Pihl M, et al. Bacterial interactions with nanostructured surfaces. *Curr Opin Colloid Interface Sci*. 2018;*38*:170-189.
13. Brunette DM. Fibroblasts on micromachined hierarchically substrata orient to grooves of different dimensions. *Exp Cell Res*. 1986;*164*:11-26.
14. Mussig E, Schulz S, Spatz JP, Ziegler N, Tomakidi P, Steinberg T. Soft micropillar interfaces of distinct biomechanics govern behaviour of periodontal cells. *Eur J Cell Biol*. 2010;*89*:315-325.
15. Weiss P. Experiments on cell and axon orientation in vitro: the role of colloidal exudates in tissue organization. *J Exp Zool*. 1945;*100*:353-386.
16. Chehroudi B, Gould TR, Brunette DM. Titanium-coated micromachined grooves of different dimensions affect epithelial and connective-tissue cells differently in vivo. *J Biomed Mater Res*. 1990; *24*:1203-1219.
17. Chehroudi B, Gould TR, Brunette DM. Effects of a grooved epoxy substratum on epithelial cell behavior in vitro and in vivo. *J Biomed Mater Res*. 1988;*22*:459-473.
18. Clark P, Connolly P, Curtis ASG, Dow JAT, Wilkinson DW. Topographical control of cell behaviour: II. Multiple grooved substrata. *Development*. 1990;*108*:635-644.
19. Lee H-J, Lee J, Lee J-T, et al. Microgrooves on titanium surface affect peri-implant cell adhesion and soft tissue sealing; an in vitro and in vivo study. *J Periodontal Implant Sci*. 2015;*45*:120-126.
20. Park J-A, Leesungbok R, Ahn S-J, Lee S-W. Effect of etched microgrooves on hydrophilicity of titanium and osteoblast responses: a pilot study. *J Adv Prosthodontics*. 2010;*2*:18-24.
21. Kim S-Y, Oh N, Lee M-H, Kim S-E, Leesungbok R, Lee S-W. Surface microgrooves and acid etching on titanium substrata alter various cell behaviors of cultured human gingival fibroblasts. *Clin Oral Implants Res*. 2009;*20*:262-272.
22. Lee S-W, Kim S-Y, Rhyu I-C, Chung W-Y, Leesungbok R, Lee K-W. Influence of microgroove dimension on cell behavior of human gingival fibroblasts cultured on titanium substrata. *Clin Oral Implants Res*. 2009;*20*:56-66.
23. Chang SS, Guo W-h, Kim Y, Wang Y-l. Guidance of cell migration by substrate dimension. *Biophys J*. 2013;*104*:313-321.
24. Teixeira AI, Abrams GA, Bertics PJ, Murphy CJ, Nealey PF. Epithelial contact guidance on well-defined micro- and nanostructured substrates. *J Cell Sci*. 2003;*116*:1881-1892.
25. Yoshinari M, Matsuzaka K, Inoue T, Oda Y, Shimono M. Effects of multigrooved surfaces on fibroblast behavior. *J Biomed Mater Res A*. 2003;*65A*:359-368.
26. Oakley C, Jaeger NA, Brunette DM. Sensitivity of fibroblasts and their cytoskeletons to substratum topographies: topographic guidance and topographic compensation by micromachined grooves of different dimensions. *Exp Cell Res*. 1997;*234*:413-424.
27. Crouch AS, Miller D, Luebke KJ, Hu W. Correlation of anisotropic cell behaviors with topographic aspect ratio. *Biomaterials*. 2009;*30*:1560-1567.
28. Brunette DM, Hamilton DW, Chehroudi B, Waterfield JD. Update on improving the bio-implant interface by controlling cell behaviour using surface topography. *Int Congr Ser*. 2005;*1284*:229-238.
29. Doll PW, Semperowitsch C, Häfner M, Ahrens R, Spindler B, Guber AE. Fabrication of micro structured dental implant abutments for optimized soft tissue integration. *Curr Dir Biomed Eng*. 2018;*4*: 677-680.
30. Pieuchot L, Marteau J, Guignandon A, et al. Curvotaxis directs cell migration through cell-scale curvature landscapes. *Nat Commun*. 2018;*9*:3995-4008.
31. Engler AJ, Sen S, Sweeney HL, Discher DE. Matrix elasticity directs stem cell lineage specification. *Cell*. 2006;*126*:677-689.
32. van Beurden HE, Snoek PAM, von der Hoff JW, Torensma R, Kuijpers-Jagtman A-M. Fibroblast subpopulations in intra-oral wound healing. *Wound Repair Regen*. 2003;*11*:55-63.
33. Li L, He Y, Zhao M, Jiang J. Collective cell migration: implications for wound healing and cancer invasion. *Burns & Trauma*. 2013;*1*:21-26.

34. Tomakidi P, Schulz S, Proksch S, Weber W, Steinberg T. Focal adhesion kinase (FAK) perspectives in mechanobiology: implications for cell behaviour. *Cell Tissue Res*. 2014;*357*:515-526.

35. Usami Y, Ishida K, Sato S, et al. Intercellular adhesion molecule-1 (ICAM-1) expression correlates with oral cancer progression and induces macrophage/cancer cell adhesion. *Int J Cancer*. 2013;*133*: 568-578.

36. Doll PW, Doll C, Käßer L, et al. Rotational UV-lithography using flexible chromium-coated polymer masks for the fabrication of microstructured dental implant surfaces: a proof of concept. *J Micromech Microeng*. 2020;*30*:45008.